ISSN 1027-4510, Journal of Surface Investigation. X-ray, Synchrotron and Neutron Techniques, 2013, Vol. 7, No. 2, pp. 211–217. © Pleiades Publishing, Ltd., 2013.
Original Russian Text © A.V. Bakaev, D.A. Terent'ev, E.E. Zhurkin, P.Yu. Grigor'ev, 2013, published in Poverkhnost'. Rentgenovskie, Sinkhrotronnye i Neitronnye Issledovaniya, 2013, No. 3, pp. 17–24.

Molecular Dynamics Simulation of the Interaction of Dislocations with Radiation-Induced Defects in Fe–Ni–Cr Austenitic Alloys

A. V. Bakaev[a, b], D. A. Terent'ev[b], E. E. Zhurkin[a], and P. Yu. Grigor'ev[a]

[a] *St. Petersburg State Polytechnic University, St. Petersburg, 195251 Russia*

[b] *SCK·CEN, Belgian Nuclear Research Center, Mol, BE-2400 Belgium*

Received July 17, 2012

Abstract—A classical molecular dynamics method is used to theoretically study the interaction of dislocations with typical radiation-induced defects in an $Fe–Ni_{10}–Cr_{20}$ austenitic alloy. As a result, a set of interactions and the corresponding values for the critical stress required for unpinning of a dislocation from an obstacle are obtained for different temperatures and interaction geometries.

DOI: 10.1134/S1027451013020067

INTRODUCTION

Austenitic steels 304L and 316L (Russian analogs are 03Kh18N11 and 03Kh16N15M3, respectively) are being used as construction materials for a number of components in the active zone of nuclear reactors. Their application is determined by good performance characteristics (strength, plasticity, corrosion resistance, etc.). However, while in service, the materials are subject to radiation-induced embrittlement caused by the accumulation and growth of radiation defects due to the effect of a fast neutron flux on the material [1]. As shown in a series of experimental works [2–4], for austenitic steels 304L and 316L the dominant type of defects arising from neutron irradiation are Frank dislocation loops, mainly of the interstitial type.

A physical mechanism for radiation hardening and embrittlement is the interaction of radiation-induced defects (Frank loops in the case of austenitic steels) with moving dislocations. The radiation-induced defects act as barriers that hinder the motion of dislocations in their slip planes, and thus, cause an increase of the yield stress of the material [5]. Being by nature dislocation defects, Frank loops enter into dislocation reactions with mobile dislocations, as a result of which the loops can be absorbed, in turn leading to the appearance of regions free from radiation defects, and the material becomes inhomogeneous. The existence of these regions can cause localized plastic deformation, which is accepted to be the reason for premature embrittlement of the material [6]. Therefore, studying the interaction of mobile dislocations with Frank loops is necessary for the understanding of plastic deformation processes in irradiated austenitic steels and the possible prediction of their premature embrittlement.

Experimental investigations of the effect of fast-neutron irradiation followed by sample analysis are extremely expensive. Sometimes accelerated ion irradiation is used in practice to imitate the effect of fast neutrons on materials [1, 7] because in this case, it is possible to avoid residual radioactivity of the samples being studied and thus, to somewhat simplify the experiment. However, this complicates the interpretation of the results of analyzing these effects. Moreover, the typical sizes of dislocation loops found in irradiated austenitic steels [2–4] are 1–50 nm, which substantially limits the feasibility of experimental study of the interaction between dislocations and these defects. Therefore, there is a necessity in alternative methods for investigating the plastic deformation of irradiated materials. Atomistic numerical simulation is now considered a promising method for gaining additional information on the effect of irradiation on the properties of materials on the atomic distance scale [8, 9].

The classical molecular dynamics (MD) method is a powerful tool for studying the interaction of dislocations with defects, which allows the investigation of rather large crystals and the variation of external load conditions [5, 9]. The interaction of dislocations with radiation-induced defects has already been studied in pure metals, such as aluminum, nickel, and copper that have the face-centered cubic (fcc) crystal lattice [10–13]. However, 03Kh18N11 austenitic alloys (also possessing the fcc lattice) are characterized by a low value of the stacking fault energy (SFE) (~20 mJ/m^2) and a relatively high elasticity modulus ($G = 80$ GPa), which is not observed in any of the pure fcc materials.

Consequently, it is essential to additionally study the effect of a high concentration of alloying elements for the above combination of SFE and G values on the

main results previously obtained for pure fcc materials. It is also necessary to study the features of the interactions between dislocations and Frank loops in alloys with properties corresponding to austenitic steels. Since the main alloying components of 03Kh18N11 stainless austenitic steel are nickel and chromium, the $Fe-Ni_{10\%}-Cr_{20\%}$ alloy can be used as a model alloy to examine the properties of these steels.

The aim of this work is the atomistic study of the interaction of screw dislocations with Frank loops in the model $Fe-Ni_{10\%}-Cr_{20\%}$ alloy by means of the classical MD method. In particular, upon varying the size of the defect within 2–5 nm at different temperatures of the material ($T = 300$–900 K), we performed the simulation of the interaction between a screw dislocation and a Frank loop. As a result, we characterized the interaction mechanisms and calculated the critical stress required for dislocations to unpin from the obstacles depending on load conditions.

SIMULATION PROCEDURE

In this work, we used the classical MD method [14] with a many-body interatomic potential based on the embedded atom model [15]. The potential used [16] was specially developed and optimized for the atomistic simulation of the mechanical properties of model austenitic Fe–Ni–Cr alloys with low SFE and high G.

The dislocation was simulated within the periodic dislocation model [17]. The X, Y, and Z Cartesian coordinates parallel to the faces of the model crystal were oriented along the [110], $[\bar{1}1\bar{2}]$, and $[\bar{1}11]$ crystallographic directions respectively. Periodic boundary conditions were applied along the X and Y axes. The $(\bar{1}11)$ planes of the box faces were free surfaces perpendicular to the Z axis. The model-crystal dimensions were $113.1a_0 \times 121.9a_0 \times 27.7a_0$ (where a_0 is the lattice constant equal to 3.52196 Å), with the crystal consisting of about 1.5 millions of atoms. The time-step of integration of the equation of atom motion was 5 fs.

The external load was implemented by a stepwise shift of a few upper atomic $(\bar{1}11)$ planes of the model crystal along the [110] direction. In these layers, the atoms are rigidly fixed in their positions, and the integration of Newton equations is not performed for them. The external loading rate (applied by shearing) was $30 \times 10^6\ s^{-1}$, which corresponds to a rate of dislocation motion of 50 m/s. Atoms in the lower layers of the crystal were also rigidly fixed in their initial positions, and the resulting shear stress caused by the shift of the upper layers of the crystal was determined based on calculating the force acting on the lower fixed layer of atoms in the direction of the applied load.

In the work, we considered the motion of a screw dislocation with a 1/2 [110] Burgers vector in the $(\bar{1}11)$ slip plane in a crystal containing a Frank loop with a 1/3 [111], 1/3 $[11\bar{1}]$ or 1/3 $[1\bar{1}1]$ Burgers vector and (111), $(11\bar{1})$ or $(1\bar{1}1)$ habit planes, respectively. We analyzed the cases when the dislocation and the Frank loop approached each other as the dislocation moved along the $[\bar{1}1\bar{2}]$ direction and the cases of reverse motion of the dislocation along the $[1\bar{1}2]$ direction. All dislocation loops were considered in the interstitial configuration. They were implemented in the model crystal by introducing fragments of atomic planes in the form of a disc with regard to the corresponding orientation of the Burgers vector.

For the atomic configurations containing a dislocation and a Frank loop we carried out a relaxation procedure (crystal energy minimization) at zero temperature, and then the configuration obtained was used as the initial configuration for the MD simulation at final temperatures of $T = 300$, 600, and 900 K. The temperature of the model crystal was initialized by assigning a velocity to each of the atoms, according to the following procedure. Primarily, momenta were given to all atoms of the system in accordance with the Maxwell distribution for the temperature $2 \times T$ (where T is the required temperature), and then the total momentum of the system was calculated, after which all velocities were simultaneously recalculated so that the total momentum of the system was zero. In order to establish dynamic equilibrium we used the following procedure: over 10000 time steps the equations of motion were integrated and for every 100 steps the momenta of all atoms were reformed so that the total kinetic energy of the system corresponded to the desired temperature. After this the procedure of external-load application was implemented according to the above algorithm.

The dislocation density was $2.387 \times 10^{15}\ m^{-2}$. The diameter of the considered loops containing 55 and 367 interstitial atoms was 2 and 5 nm, respectively. From the geometric dimensions of the modeled box, the loop density was reasoned to be $6 \times 10^{22}\ m^{-3}$. Such values of the diameter and loop density are typical for the radiation-induced defects observed experimentally in austenitic steels [3, 4].

In analysis of the final atomic configuration, we employed the numerical procedure of the linked-cell method providing the most effective search for the nearest neighbors of each atom in the model crystal [14]. The atoms of the dislocation core and the stacking fault were analyzed according to several criteria: coordination number, number of nearest neighbors of the atom corresponding to the fcc structure, and the potential energy of each atom. The configuration of the local environment of each atom was compared with the ideal fcc lattice based on the number of neighbors corresponding to the fcc structure. The atoms shown in the figures presented below have less than 12 neighboring atoms whose configuration corresponds to the fcc structure. The atoms of the disloca-

Yield stress during the motion of a dislocation in an $Fe–Ni_{10}–Cr_{20}$ alloy at different temperatures in the absence of radiation defects and the average values of the maximum applied stress (minus the yield stress) for a dislocation unpinning from the Frank loop depending on the loop size and the temperature. The yield stress was calculated by averaging the resulting shear stress over the time of 600 fs.

Temperature, K	Yield stress, MPa	Frank loop size, nm	Average value of the maximum applied stress, MPa
300	121	2	131
		5	298
600	86	2	100
		5	235
900	66	2	85
		5	193

tion core were identified by the presence of 10 or 11 neighbors; the stacking fault was shown as a double layer of atoms having 9 neighbors.

The maximum values of the applied stress required for the moving dislocation to overcome the Frank loop σ_{max} were obtained from an analysis of the averaged values of the instantaneous load stress $\sigma(t)$. The time interval for averaging $\sigma(t)$ was 500 fs.

RESULTS AND DISCUSSION

By means of numerical MD simulation we obtained the yield stress σ_Y for the motion of a screw dislocation with the 1/2 [110] Burgers vector in the ideal crystal (defect-free). These values are given in Table 1. It should be noted that the yield stress decreases nonlinearly with an increase in the temperature: when the temperature is three times greater (from 300 to 900 K) the σ_Y value is two times smaller.

Then we considered the model crystals containing a Frank loop. We analyzed 36 dislocation reactions between the screw dislocation with the 1/2 [110] Burgers vector (split into two partial dislocations with 1/6 [211] and 1/6 $[12\bar{1}]$) Burgers vectors) moving in the $(\bar{1}11)$ slip plane and the Frank loops with the 1/3 [111], 1/3 $[11\bar{1}]$, and 1/3 $[1\bar{1}1]$ Burgers vectors at temperatures of $T = 300$, 600, and 900 K for two possible directions of approach: $[\bar{1}1\bar{2}]$ and $[1\bar{1}2]$.

It is found that all dislocation reactions can be divided into five main groups by the interaction type.

1. Absorption of the Frank Loop (with the Burgers Vector $\mathbf{b} = 1/3\ [111]$*) with the Emission of a Perfect Loop (*$\mathbf{b} = 1/2\ [110]$*)*

Under the action of an applied external load, partial dislocations slip towards the loop and the leading dislocation interacts with the nearest segment of the loop (Fig. 1a), causing splitting of the upper half of the loop. Then the leading partial dislocation continues to advance and reaches the far point of the loop, after which the stacking fault of the upper half of the loop starts to be removed, resulting in the formation of a set of intrinsic stacking faults in different planes of the {111} type (Fig. 1b). The configuration formed is static in the $(\bar{1}11)$ plane, and the trailing partial dislocation moving forward is connected to the loop that transformed into a set of intrinsic stacking faults. As a result of the reaction, a helical turn forms (Fig. 1c), which is emitted as a perfect loop with a 1/2 [110] Burgers vec-

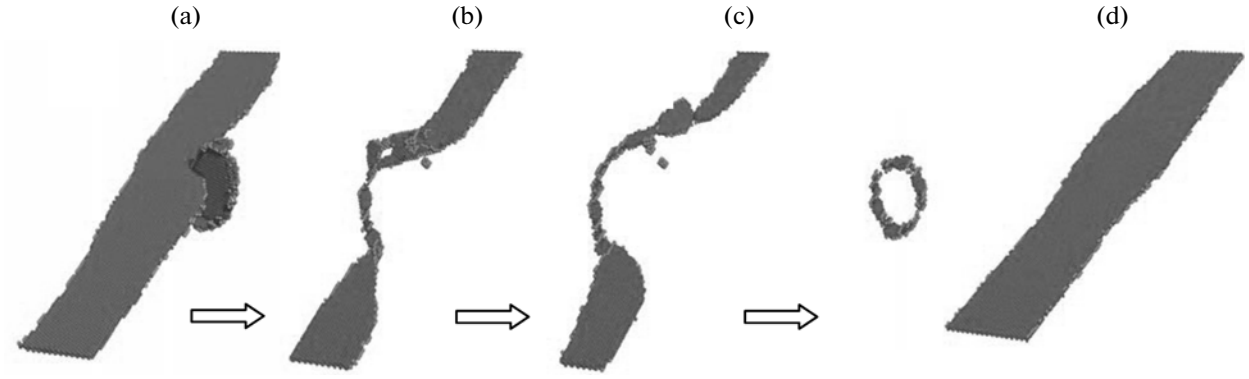

Fig. 1. Visualization of the type-1 dislocation reaction characterizing the interaction of a screw dislocation and a Frank loop with a diameter of 5 nm and the Burgers vector $\mathbf{b}_L = 1/3\ [111]$ at a temperature of $T = 300$ K at the times (a) 150 ps, (b) 300 ps, (c) 450 ps, and (d) 600 fs after the simulation onset.

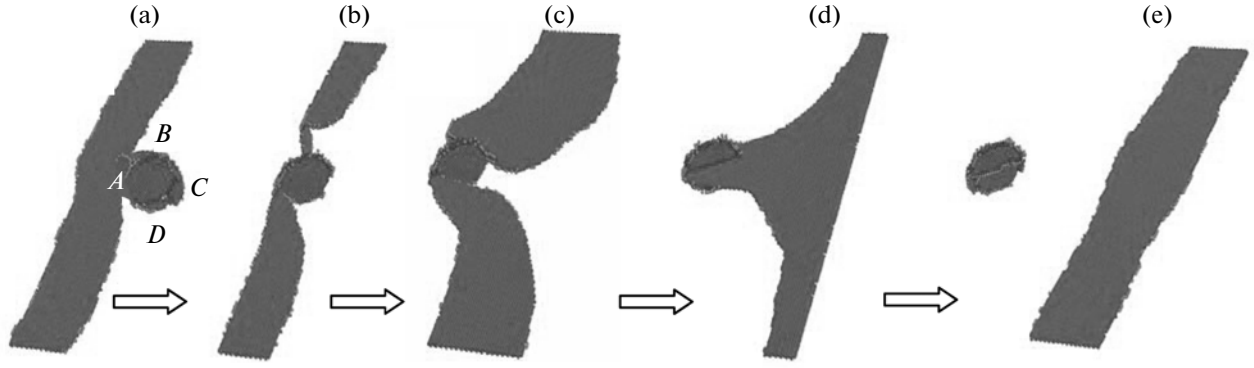

Fig. 2. Visualization of the type-2 dislocation reaction with a loop with the Burgers vector $\mathbf{b}_L = 1/3\,[11\bar{1}]$. Visualizations at the times (a) 150 ps, (b) 300 ps, (c) 450 ps, (d) 600 fs and (e) 750 ps after the simulation onset are shown. $T = 300$ K.

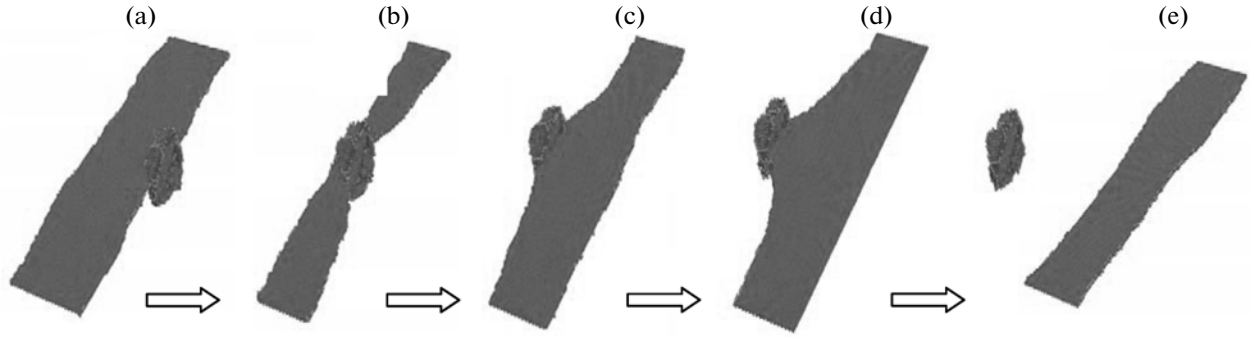

Fig. 3. Visualization of the type-3 dislocation reaction with a loop with the Burgers vector $\mathbf{b}_L = 1/3[1\,\bar{1}\,1]$. Visualizations at the times (a) 125 ps, (b) 250 ps, (c) 375 ps, (d) 500 ps, (e) and 625 ps after the simulation onset are shown. $T = 300$ K.

tor (Fig. 1d) as a result of the closing of the dislocation under the action of increasing stress.

2. Partial Dislocations Cause a Shear of the Loop

Initially, the dislocation is repelled from the loop, however, under the action of increasing load stress it approaches the loop and forms a constriction at the point *A* (Fig. 2a). Then the dislocation is split at this point in the transverse $(1\bar{1}1)$ slip plane and moves downward along the *AD* side. Then it is again split in the initial slip plane, interacting with the segment *D* (Fig. 2b). As a result of the interaction, the left half of the moving dislocation contains a segment that cannot slip in the $(\bar{1}11)$ plane, therefore the free segment of the dislocation starts to bow under the action of increasing stress (Fig. 2c). A dislocation dipole forms, and the leading partial dislocation closes, continuing to advance, while the trailing partial dislocation remains attached to the loop (Fig. 2d). At the moment when the maximum critical stress is reached, the trailing partial dislocation detaches from the loop, leaving a step on its surface (Fig. 2e).

3. Partial Dislocations Traverse the Loop

Initially, the leading partial dislocation is attracted to the loop (Fig. 3a) and joins it. Then, under the action of external load, the trailing partial dislocation also approaches the loop (Fig. 3b), thus causing detachment of the leading partial dislocation (Fig. 3c) because the leading and trailing dislocations repel each other. Under the action of stress, the leading partial dislocation continues to advance (Fig. 3d), while at the same time, the trailing dislocation interacts with the loop by attaching to it. Then the continued application of external load results in an increase in the stress, and when its maximum value is reached, the trailing partial dislocation detaches (Fig. 3e).

4. Absorption of the Loop with the Formation of Two Mobile Superjogs

First, the leading partial dislocation is attracted to the loop (Fig. 4a), moving towards the plane containing the loop. Then the leading dislocation is re-split in this plane (Fig. 4b), thus removing the stacking fault inside the loop, which transforms the Frank loop into a perfect loop. However, during this transformation, the upper and lower halves of the loop (steps) form

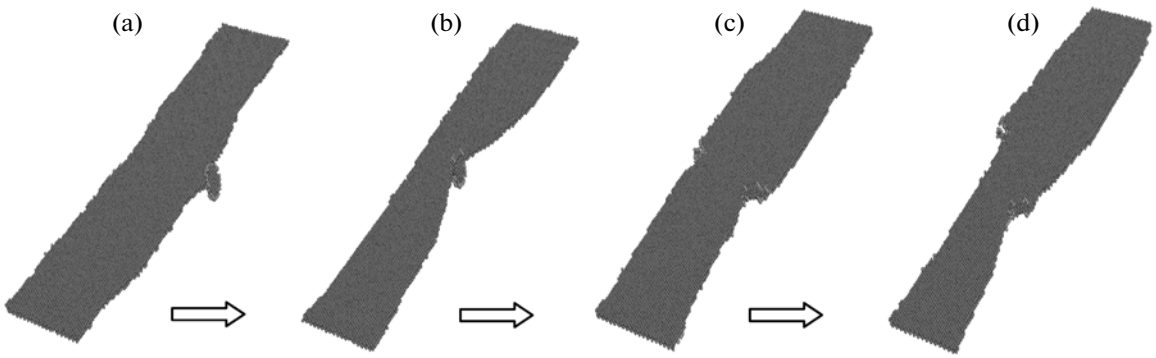

Fig. 4. Visualization of the type-4 dislocation reaction with a loop with a diameter of 2 nm and the Burgers vector $\mathbf{b}_L = 1/3[1\,\bar{1}\,1]$ at the temperature $T = 900$ K. Visualizations at the times (a) 100 ps, (b) 200 ps, (c) 300 ps and (d) 400 ps after the simulation onset are shown.

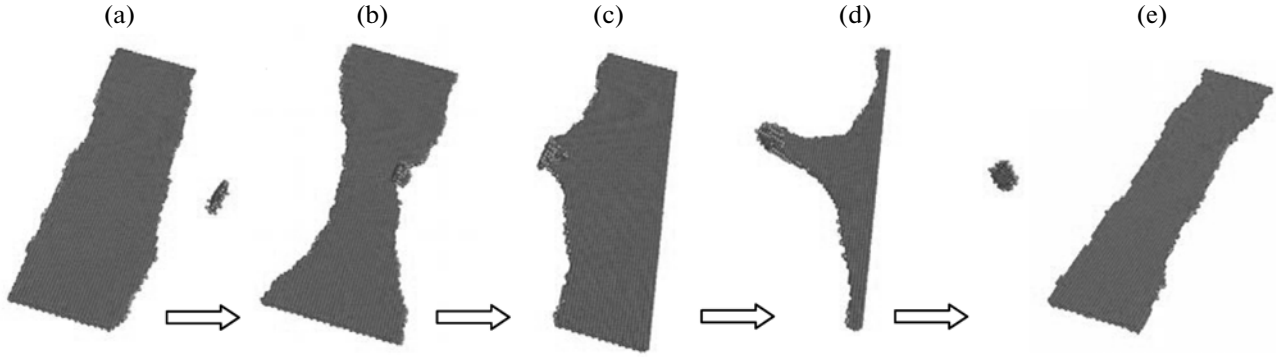

Fig. 5. Visualization of the type-5 dislocation reaction with a loop with a diameter of 2 nm and the Burgers vector $\mathbf{b}_L = 1/3\,[1\,\bar{1}\,1]$. Visualizations at the times (a)150 ps, (b) 300 ps, (c) 450 ps, (d) 600 ps and (e) 750 ps after the simulation onset are shown $T = 300$ K.

half-loops with Burgers vectors of $1/2\,[01\,\bar{1}]$ and $1/2\,[110]$ (Fig. 4c). These half-loops attach to the leading and trailing partial dislocations in the form of steps and they together continue to move because both Burgers vectors are in the $(1\,\bar{1}\,1)$ plane (Fig. 4d). As a result of the above interactions, the dislocation loop is completely absorbed.

5. Loop Regeneration Occurs in Another (111) Plane

The leading partial dislocation is attracted to the loop and interacts with the nearest segment (Fig. 5a, b), causing splitting of the upper half of the loop, as in the case of reaction 1. The leading partial dislocation continues to move (Fig. 5c); the trailing partial dislocation approaching the loop causes splitting (Fig. 5d) of the lower half of the loop, thus again generating (Fig. 5e) the interstitial Frank loop in another (111) habit plane.

Figures 6a and 6b show the maximum values of the applied stress σ_{max} (minus the corresponding values of the yield stress) required for the dislocation to pass through a Frank loop with a diameter of 2 nm (a) and 5 nm (b) respectively for all 36 considered dislocation reactions. From the diagrams depicted in Fig.6 it is seen that the largest values of the applied stress σ_{max} are required to perform reactions accompanied by the absorption of the loop. The lowest σ_{max} value is required for the dislocation to unpin from a Frank loop according to the reaction of the intersection of dislocation loop (type 3).

For a loop with a diameter of 2 nm, the lowest σ_{max} value corresponds to the passing of the dislocation through the loop according to reactions 3 and 4. Similarly, for a loop with a diameter of 5 nm, the least stress σ_{max} was applied in type 3 reactions. The σ_{max} values averaged over the considered interaction configurations (at the same temperature and loop size) are listed in Table 1 and shown in Figs. 6a and 6b by the dashed line. The loop size affected the spread in σ_{max} values around the above averaged values. Here the ratio between the largest and smallest σ_{max} values was two for a loop with a diameter of 2 nm and three for a loop with a diameter of 5 nm. The loop size also

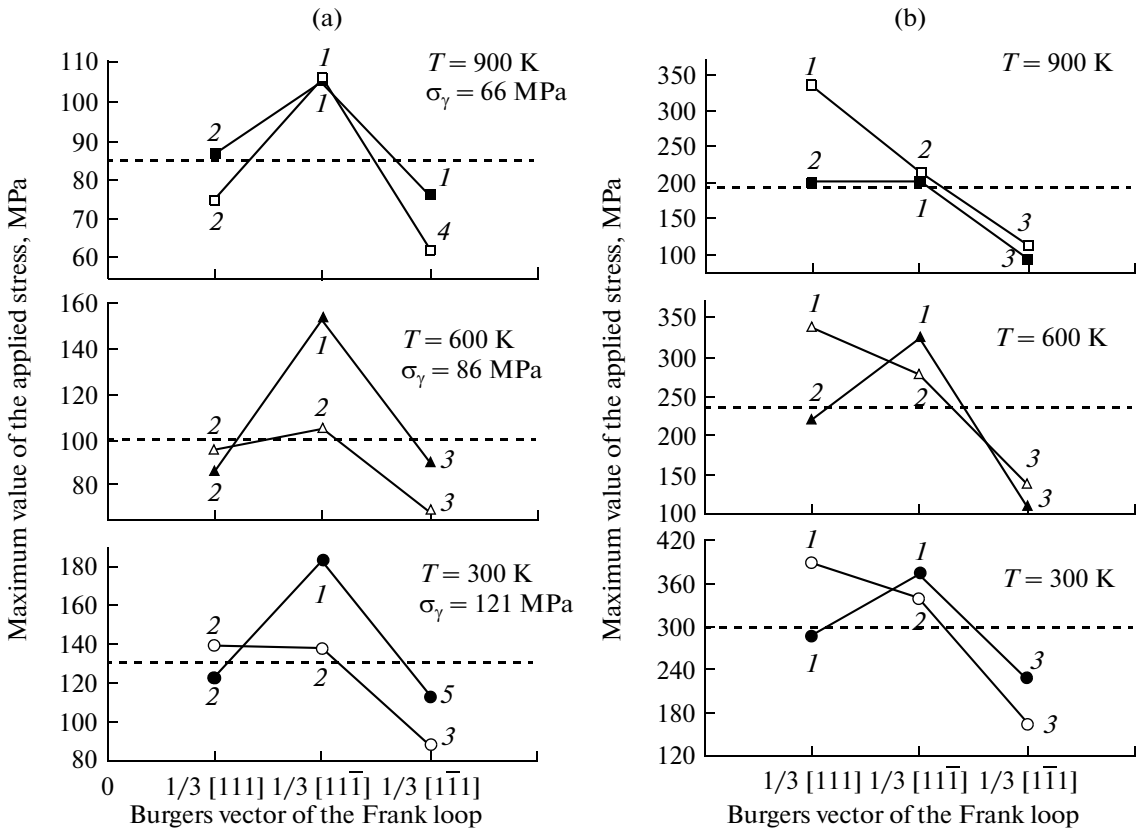

Fig. 6. Diagrams showing the maximum values of the applied stress (minus the yield stress) required for a screw dislocation to overcome Frank loops with a diameter of (a) 2 nm and (b) 5 nm depending on the temperature of the material, Burgers vector of the loop, and the direction of the dislocation motion. The dashed lines denote the average values of the maximum applied stress in each of the presented diagrams where the temperature and the direction of the dislocation motion are fixed. Unshaded markers denote the motion of the dislocation along the $[\bar{1}1\bar{2}]$ direction; shaded markers denote the motion along the $[1\,\bar{1}2]$ direction. Figures near each marker denote the type of dislocation–Frank loop interaction. Panel (a) shows the yield stress σ_Y when the dislocation moves in the absence of radiation-induced defects.

affected the type of dislocation reaction in 8 out of 18 considered interactions (at two loop sizes with other parameters being equal). For example, when a dislocation moves in the $[1\,\bar{1}2]$ direction at a temperature of 300 K and the loop diameter is 2 nm, a type-2 reaction occurs, with other parameters being equal, but at a loop diameter of 5 nm this is a type-1 reaction. Hence, the conclusion can be drawn that, for estimating the contribution of dislocation loops to radiation hardening, it is important to take into account the interaction geometry and possible inhomogeneous loop distribution in the material.

As expected, the average σ_{max} value decreases with an increase in the temperature of the material (Table 1). In most cases (24 reactions out of 36), an increase in the temperature did not change the type of dislocation reaction. It is found that for the interaction of a loop with a $1/3\,[1\,\bar{1}1]$ Burgers vector, temperature is important for the determination of the type of dislocation reaction: a type-5 reaction corresponded to the $[1\,\bar{1}2]$ direction of the dislocation motion at a temperature of $T = 300$ K and a loop diameter of 2 nm; at $T = 600$ K, a type-3 reaction; at $T = 900$ K, a type-1 reaction. Thus, the interaction mechanism (as well as the corresponding σ_{max} value) strongly depends on the temperature for one-third of the interaction configurations considered.

CONCLUSIONS

As a result of the study performed, the yield stress was calculated for the motion of a dislocation (in the absence of radiation-induced defects) at different temperatures. Furthermore, we analyzed the dislocation reactions between Frank loops and dislocations depending on the temperature of the material, loop sizes and orientation relative to the dislocation. According to the results of analysis of the defect–dislocation interaction, the following five types of reactions were observed:

(i) Absorption of the Frank loop (**b** = 1/3 [111]) with the emission of a perfect loop (**b** = 1/2 [110]).

(ii) Partial dislocations cause a shear of the loop (with a constriction formed by partial dislocations).

(iii) Partial dislocations intersect the loop (without a constriction formed by partial dislocations).

(iv) Absorption of the loop with the formation of two mobile superjogs.

(v) Loop regeneration occurs in another (111) plane.

The maximum values of the applied external stress σ_{max} required for the dislocation to pass through a rectangular network of identical obstacles (Frank loops) are found. The largest σ_{max} value is necessary for the reaction to proceed with the formation of a helical turn, i.e., the transformation reaction of the Frank loop into a perfect loop. The smallest σ_{max} value was determined for the reaction with the loop intersected by partial dislocations. The loop size is found to affect the spread of σ_{max} values relative to the averaged (over the interaction direction and the Burgers vector of the loop) σ_{max} values. The ratio between the largest and smallest σ_{max} values was two for a loop with a diameter of 2 nm and three for a loop with a diameter of 5 nm. In 8 out of 18 dislocation reactions the loop size also affected the type of dislocation reaction. As the temperature of the material increases, the average σ_{max} value decreases. The temperature of the material also affects the interaction mechanism (and correspondingly, the σ_{max} value) in one-third of the interaction configurations considered.

Thus, the conclusion can be drawn that in order to estimate the contribution of dislocation loops to radiation hardening, it is essential to take into account the interaction geometry of a possible inhomogeneous loop distribution and the temperature of the material.

ACKNOWLEDGMENTS

The work was supported by the Ministry of Education and Science of the Russian Federation within the Federal Target Program "Human Capital for Science and Education in Innovative Russia" for 2009–2013.

REFERENCES

1. S. W. Gary, *Fundamentals of Radiation Materials Science: Metals and Alloys* (Springer, Berlin, Heidelberg, New York, 2007).
2. S. J. Zinkle, P. J. Maziasz, and R. E. Stoller, J. Nucl. Mater. **206**, 266 (1993).
3. C. Pokor and Y. Brechet, J. Nucl. Mater. **326**, 19 (2004).
4. C. Pokor and Y. Brechet, J. Nucl. Mater. **326**, 30 (2004).
5. D. J. Bacon, *Introduction to Dislocations*, 4th ed. (Butterworth-Heinemann, 2001).
6. Xiaoqiang Li and A. Almazouzi, J. Nucl. Mater. **385**, 329 (2009).
7. G. V. Lysova, G. A. Birzhevoi, and A. M. Dvoryashin, J. Surf. Invest. **5**, 396 (2011).
8. V. A. Kirsanov, *Computer Experiment in Atomic Material Science* (Energoatomizdat, Moscow, 1990) [in Russian].
9. D. Terentyev, D. J. Bacon, and Yu. N. Osetsky, Philos. Mag. **90**, 1019 (2010).
10. T. Nogaret, C. Robertson, and D. Rodney, Philos. Mag. **87**, 945 (2007).
11. D. Rodney and G. Martin, Phys. Rev. B **61**, 8714 (2000).
12. D. Rodney, Acta Mater. **52**, 607 (2004).
13. Y. N. Osetsky, D. Rodney, and D. J. Bacon, Philos. Mag. **86**, 2295 (2006).
14. M. P. Allen and D. J. Tildesley, *Computer Simulations of Liquids* (Clarendon, Oxford, 1987).
15. M. S. Daw and M. I. Baskes, Phys. Rev. B **29**, 6443 (1984).
16. G. Bonny, D. Terentyev, R. C. Pasianot, et al., Model. Simulation Mater. Sci. Eng. **19**, 085008 (2011).
17. Y. N. Osetsky and D. J. Bacon, Model. Simulation Mater. Sci. Eng. **11**, 427 (2003).